Taylor & Francis
Taylor & Francis Group

ORIGINAL RESEARCH

🔓 OPEN ACCESS | Check for updates

Synergistic anti-tumor efficacy of oncolytic influenza viruses and B7-H3 immune-checkpoint inhibitors against IC-resistant lung cancers

Dörthe Masemann[a,b], Ramona Meissner[a,b], Tanja Schied[b], Brian D Lichty[c], Ulf R Rapp[d], Viktor Wixler[a,b], and Stephan Ludwig 🆔[a,b]

[a]Cells in Motion" Interfaculty Center (Cimic), University of Muenster, Muenster, Germany; [b]Center for Molecular Biology of Inflammation, Institute of Virology, University of Muenster, Muenster, Germany; [c]Department of Pathology and Molecular Medicine, McMaster Immunology Research Centre, McMaster University, Hamilton, Ontario, Canada; [d]Department of Lung Development and Remodelling, Max Planck Institute for Heart and Lung Research, Bad Nauheim, Germany

ABSTRACT

Non-small cell lung cancers (NSCLCs) establish a highly immunosuppressive tumor microenvironment supporting cancer growth. To interfere with cancer-mediated immunosuppression, selective immune-checkpoint inhibitors (ICIs) have been approved as a standard-of-care treatment for NSCLCs. However, the majority of patients poorly respond to ICI-based immunotherapies. Oncolytic viruses are amongst the many promising immunomodulatory treatments tested as standalone therapy or in combination with ICIs to improve therapeutic outcome. Previously, we demonstrated the oncolytic and immunomodulatory efficacy of low-pathogenic influenza Aviruses (IAVs) against NSCLCs in immunocompetent transgenic mice with alung-specific overexpression of active Raf kinase (Raf-BxB). IAV infection not only resulted in significant primary virus-induced oncolysis, but also caused afunctional reversion of tumor-associated macrophages (TAMs) comprising additional anti-cancer activity. Here we show that NSCLCs as well as TAMs and cytotoxic immune cells overexpress IC molecules of the PD-L2/PD-1 and B7-H3 signaling axes. Thus, we aimed to combine oncolytic IAV-infection with ICIs to exploit the benefits of both anti-cancer approaches. Strikingly, IAV infection combined with the novel B7-H3 ICI led to increased levels of M1-polarized alveolar macrophages and increased lung infiltration by cytotoxic Tlymphocytes, which finally resulted in significantly improved oncolysis of about 80% of existing tumors. In contrast, application of clinically approved α-PD-1 IC antibodies alone or in combination with oncolytic IAV did not provide additional oncolytic or immunomodulatory efficacy. Thus, individualized therapy with synergistically acting oncolytic IAV and B7-H3 ICI might be an innovative future approach to target NSCLCs that are resistant to approved ICIs in patients.

Introduction

Non-small cell lung cancer (NSCLC) remains the leading cause of cancer death worldwide.[1] As research in this field progressed, interfering with cancer-immune cell interactions came to the forefront of cancer research. Immune-checkpoint inhibitors (ICI) target ligands or their respective receptors, thereby reviving suppressed cytotoxic immune responses against cancer. Thus, the use of ICIs, such as antibodies against programmed cell death 1 (PD-1) or one of its ligands (PD-L1), has been approved as standard treatment for NSCLC patients. However, impressive clinical responses are registered in only 20–30% of patients, while the vast majority do not respond to this treatment.[2] Therefore, alternative immunosuppressive molecules targetable with ICIs have attracted increasing attention. One of the highly investigated IC ligands is the recently described homolog 3 of B7.1/2 (B7-H3). Being expressed by cancer cells or TAMs, it was shown to be a potent negative regulator of cytotoxic innate and adaptive immune cells.[3–5] Monoclonal α-B7-H3 antibodies (Enoblituzumab) are currently being tested in clinical trials for their efficacy against

melanoma, squamous cell carcinoma of the head and neck and NSCLCs (*NCT02381314*). However, the response rate to therapy with α-B7-H3 ICIs is not yet known.

A low response rate to ICI immunotherapy can be explained by the complex network of several mechanistically different cancer-immune evasion strategies. In addition to overexpression of immune-checkpoint molecules, inadequate T cell infiltration or the local immunosuppression in the TME can significantly limit IC therapies. Additionally, TAMs have been described to impede the anti-cancer immunity by oppressing cytotoxic NK and T cell responses.[4,6] Hence, single application of ICIs appears not to be efficient enough to overcome the highly immunosuppressive cancer microenvironment.[7–10] In this context, oncolytic viruses (OVs) seem to be ideal candidates to synergize with ICIs as additional immunomodulatory therapeutics, having two additional advantages over ICIs. The primary virus-induced cancer cell destruction results in (i) release of tumor-associated antigens (TAAs) and (ii) critical remodeling of the tumor microenvironment (TME), thereby stimulating recruitment and activation of cytotoxic effector

CONTACT Stephan Ludwig ✉ ludwigs@uni-muenster.de 💻 Centre for Molecular Biology of Inflammation (ZMBE), Institute of Virology (IVM), Westfaelische Wilhelms-University Muenster, Von-Esmarch-Str. 56, Muenster D-48149, Germany.
🅑 Supplemental data for this article can be accessed on the publisher's website.

cells. Thus, the combined use of OVs and ICI can synergistically improve the efficacy of cancer therapies by exploiting robust anti-cancer immune responses. In fact, several preclinical studies already demonstrated the advantage of combined OV and ICI application against melanoma, breast cancer or small-cell lung carcinoma,[11–15] finally resulting in initiation of first clinical trials combining both agents for cancer therapies in patients.[16,17] However, due to heterogeneity of tumor tissues and the complexity of tumor-associated immune cell subsets, it is unlikely to identify a "one serves all" strategy. Therefore, there is an urgent need for cancer individualized therapies to improve therapeutic outcome of IC-resistant cancers.

Recently, we described an immunocompetent murine model for NSCLCs[18] that closely resembles the human cancer phenotype exhibiting a highly immunosuppressive cancer TME.[19] We demonstrated oncolytic efficacy of intranasally applied IAVs toward NSCLC. Interestingly, the oncolytic efficacy was not solely based on virus-induced cell lysis. It was complemented with polarization of tumor-associated macrophages (TAMs) to a proinflammatory anti-cancer phenotype enhancing anti-cancer immune responses. Nevertheless, an efficient cancer cell lysis and immune cell conversion was mainly detected in lung tissue areas directly infected by the virus. The tumor foci in virus-free lung areas were also affected in their number and size, but to a much lesser extent. TAM repolarization was also only partial, suggesting that immune evasion mechanisms are still maintained, restraining the full unfolding of IAV-induced anti-cancer immune cytotoxic activity.

Thus, we aimed to characterize mechanisms underlying NSCLC immune-evasion and TAMpolarization with regard to identify targetable IC molecules that might be applied with oncolytic IAVs. Combining the benefits of each immunotherapeutic approaches, synergistically promoting each other, shall overcome the resistance of NSCLCs against ICIs and boost cancer cell lytic efficacy.

Results

Non-small cell lung cancer growth results in overexpression of the inhibitory immune checkpoint molecules B7-H3 and PD-1, and accumulation of TAMs expressing increased levels of B7-H3 and PD-2

To gain comprehensive insights into acquisition of IC molecules in the lungs of NSCLCbearing Raf-BxB mice, we analyzed the expression of different IC molecules by RT-qPCR. Gene expression levels in the lungs of Raf-BxB mice were always compared to C57Bl/6 WT mice of the same age (Figure 1a). Interestingly, the recently identified immune-checkpoint ligand B7-H3 was significantly upregulated by 4-fold in Raf-BxB mice. In addition, mRNA expression levels of the well-characterized IC receptor PD-1 was also significantly increased, even though the overall lung expression levels of its ligands PD-L1 and PD-L2 were surprisingly not altered (PDL-2) or even downregulated (PD-L1) in tumor-bearing lungs compared to tumor-free WT lungs. The overall levels of neither CTLA-4 IC receptor described to be expressed by tumor-infiltrating T lymphocytes (TILs), nor its ligands CD80 and CD86 were significantly changed, indicating a minor

relevance of CTLA-4 signaling in NSCLC-mediated immune-evasion in the lungs of Raf-BxB tumor-bearing mice.

While PD-1 is described to be expressed mainly on tumor-infiltrating T lymphocytes, the expression pattern of B7-H3 is more complex, as it can be expressed by either tumor cells or TAMs. Indeed, IHC staining of B7-H3 on lung specimen of NSCLC-bearing Raf-BxB mice revealed expression of B7-H3 in cancer cells expressing the human Raf-BxB oncogene (Figure 1a), but also in additional cell types besides the Raf-BxB positive tumor foci. Staining of sequential lung sections for Siglec-F indicates that these cells are most likely alveolar macrophages (aMφ) within the cancer environment (Figure 1b, indicated by arrows). To proof this hypothesis, we analyzed IC ligands exposed on the surface of TAMs via multi-color flow cytometry. TAMs were isolated from lung tissue and alveolar macrophages of Raf-BxB mice were compared with that of WT control mice. We identified massive accumulation of TAMs of alveolar macrophage origin (CD45$^+$/CD11c$^+$/SigF$^+$) in the lungs of Raf-BxB mice (Figure 1c). Furthermore, the majority of macrophages showed decreased expression of the MHCII surface receptor, but increased levels of the macrophage mannose receptor C type 1 (MRC-1), indicating an immunosuppressed M2-phenotype, as already characterized in more detail previously.[19] Of note, the immune-checkpoint ligand B7-H3 was expressed on a significantly higher number of alveolar macrophages of Raf-BxB mice compared with WT mice (Figure 1d). Furthermore, the amount of the molecule per cell was also increased compared to WT mice, as indicated by the geoMFI (Figure 1e). Additionally, significantly increased, albeit overall low, percentages of alveolar macrophages demonstrated surface expression of PD-L2 (Figure 1d), even though the levels of molecules per cell were not altered (Figure 1e). In contrast, surface expression of PD-L1 was significantly reduced on lung-derived macrophages from NSCLC-bearing mice compared to WT controls (Figure 1d, e).

Thus, cancer cells, but also alveolar macrophages of Raf-BxB mice express increased levels of B7-H3 and PD-L2 molecules, indicating that TAMs are also involved in immune-evasion of NSCLCs, possibly via a B7-H3 and/or a PD-L2 -mediated mechanism.

Progressive NSCLC growth results in exhaustion of lung NK and T cell subsets

The expression of immune-checkpoint ligands on cancer cells and TAMs is associated with suppressed cytotoxic NK and T cell responses and correlates with poor prognoses in NSCLCpatients.[20,21] Thus, we aimed to investigate the lung immune status of innate and adaptive cytotoxic immune cell subsets.

To first gain a conclusive picture of cytotoxic immune cell functions in the lungs of NSCLCbearing Raf-BxB mice, expression of cancer immunology-related genes in the lungs of Raf-BxB mice were compared to the respective WT controls via nanoString nCounter PanCancer immune profiling. Interestingly, gene clusters involved in immune cell functions, such as adaptive immune cells, NK and T cell function and interferon responses were found to be affected in the lungs of NSCLC-bearing mice (Figure 2a). Specifically, cytotoxic cell
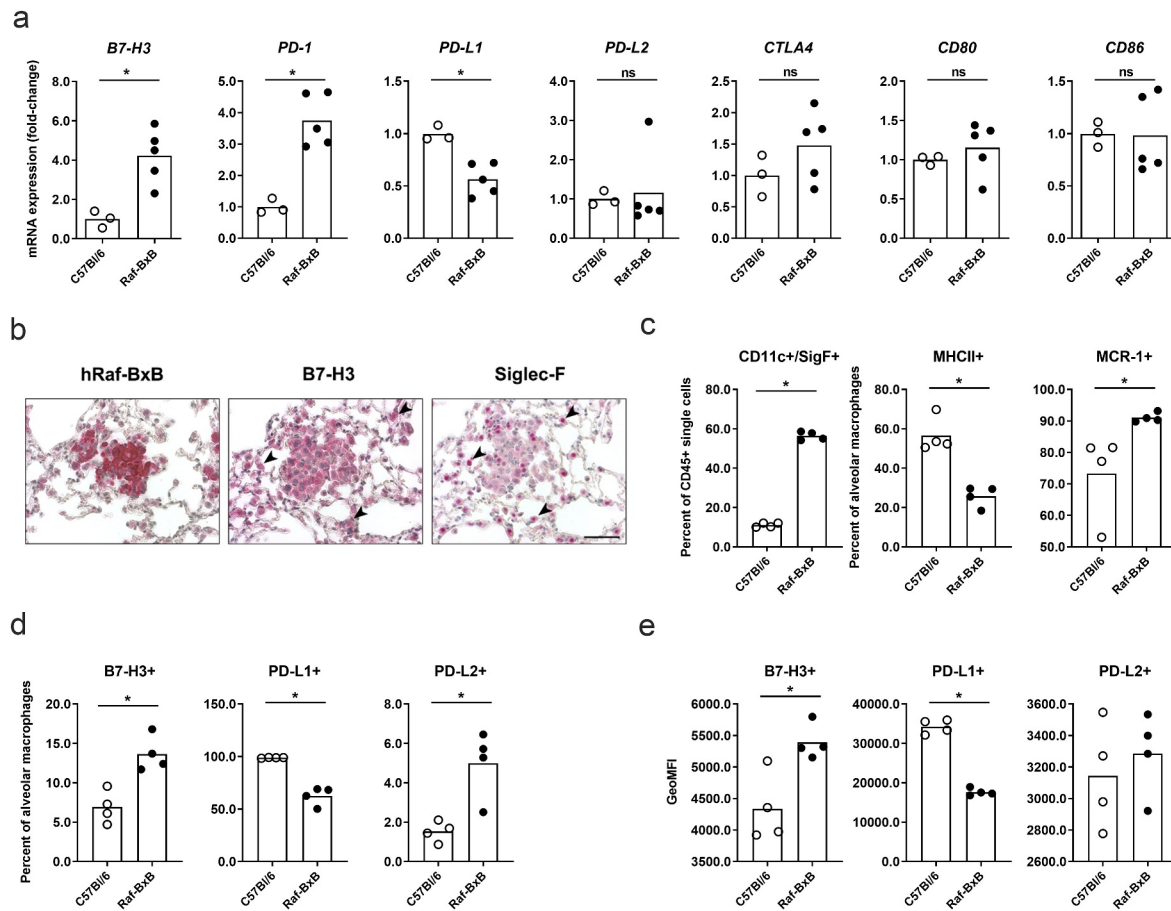
Figure 1. NSCLC growth induces overexpression of IC molecules and accumulation of immunosuppressive TAMs expressing increased levels of IC ligands. (A) Total lung lysates of C57Bl/6 WT or NSCLC-bearing Raf-BxB mice of the same age were investigated for mRNA expression levels of immune checkpoint molecules via TaqMan RT-qPCR. The values were first normalized to mRNA amounts of the housekeeping genes GAPDH and Cytochrome C and the mean value of WT mice was arbitrarily set to 1 and fold-change mRNA expression levels are presented. (B) Expression and lung-localization of human Raf-BxB oncogene and B7-H3 and Siglec-F was investigated via immunohistochemistry staining of lung sections derived from Raf-BxB mice. Bars represent 100 μm. (C-E) Lungs of C57Bl/6 and Raf-BxB mice were enzymatically processed and lung-derived single, living CD45$^+$ immune cells were investigated for levels of alveolar macrophages (CD11c$^+$/SigF$^+$) (C) and expression of the respective surface markers and IC molecules (C; D) as well as for the geometric mean fluorescence intensity (GeoMFI) of each molecule on positively stained cells (E). The detailed gating strategy is presented in Supplementary Figure 2.

scores as well as functional scores for NK cells and T lymphocytes, including cytotoxic CD8$^+$, cells were down-regulated in Raf-BxB mice (Figure 2b).

In order to verify the proposed suppression of NK- and T cell effector functions, immune cells were isolated from lungs of cancer-bearing Raf-BxB mice and WT controls and analyzed via flow cytometry for exhaustion and activation markers. The level of NK cells (CD3$^-$/Dx5$^+$) amongst all lung-derived leukocytes (CD45$^+$) was significantly lower in the lungs of Raf-BxB mice (Figure 2c). However, percentages of IFNγ-expressing NK cells expressing the immune-checkpoint receptors PD-1 and CTLA-4 were increased, while percentages of IFNγ expressing NK cells were decreased in the lungs of Raf-BxB mice. Although the differences between the few analyzed animals were not significant, the results certainly indicate toward NK cell exhaustion in tumor-bearing lungs. NK cells isolated from the lungs of RafBxB mice and C57Bl/6 WT mice were negative for B7-H3 surface expression (Figure 2c).

Like NK cells, the relative number of cytotoxic T lymphocytes (CD45$^+$/CD3$^+$/CD8$^+$) was lower in Raf-BxB

than in WT lungs, but the proportion of PD-1- and CTLA4-positive cells among them was higher in tumor-bearing lungs with simultaneously decreased number of IFN-γ$^+$activated T cells (Figure 2d). The ratio of Treg to cytotoxic T lymphocytes (T$_{cytotox}$; CD3$^+$/CD8$^+$/IFNγ$^+$) as well as CD3$^+$/CD8$^+$/PD1$^+$ to CD3$^+$/CD8$^+$/IFNγ$^+$ T lymphocytes was significantly increased in the lungs of Raf-BxB compared to C57Bl/6 WT mice (Figure 2e).

The changes in the T helper cell population (CD3$^+$/CD4$^+$) were less pronounced, but the percentages of PD-1 expressing cells were also increased and the levels of IFN-γ$^+$ cells were decreased (Figure 2f). Yet, the number of immunosuppressive Treg (CD3$^+$/CD4$^+$/Foxp3$^+$) cells was enhanced in Raf-BxB lungs. Like NK cells, both T lymphocyte subsets were negative for B7-H3 surface expression (Figure 2d, f).

Taken together, these data demonstrate a strong exhaustion of immune cell subsets in the lungs of NSCLC-bearing mice. Furthermore, the investigated cytotoxic immune cells subsets in RafBxB lungs expressed higher levels of the IC receptor PD-1, highlighting PD-L2/PD-1 as a possible ICI mechanism
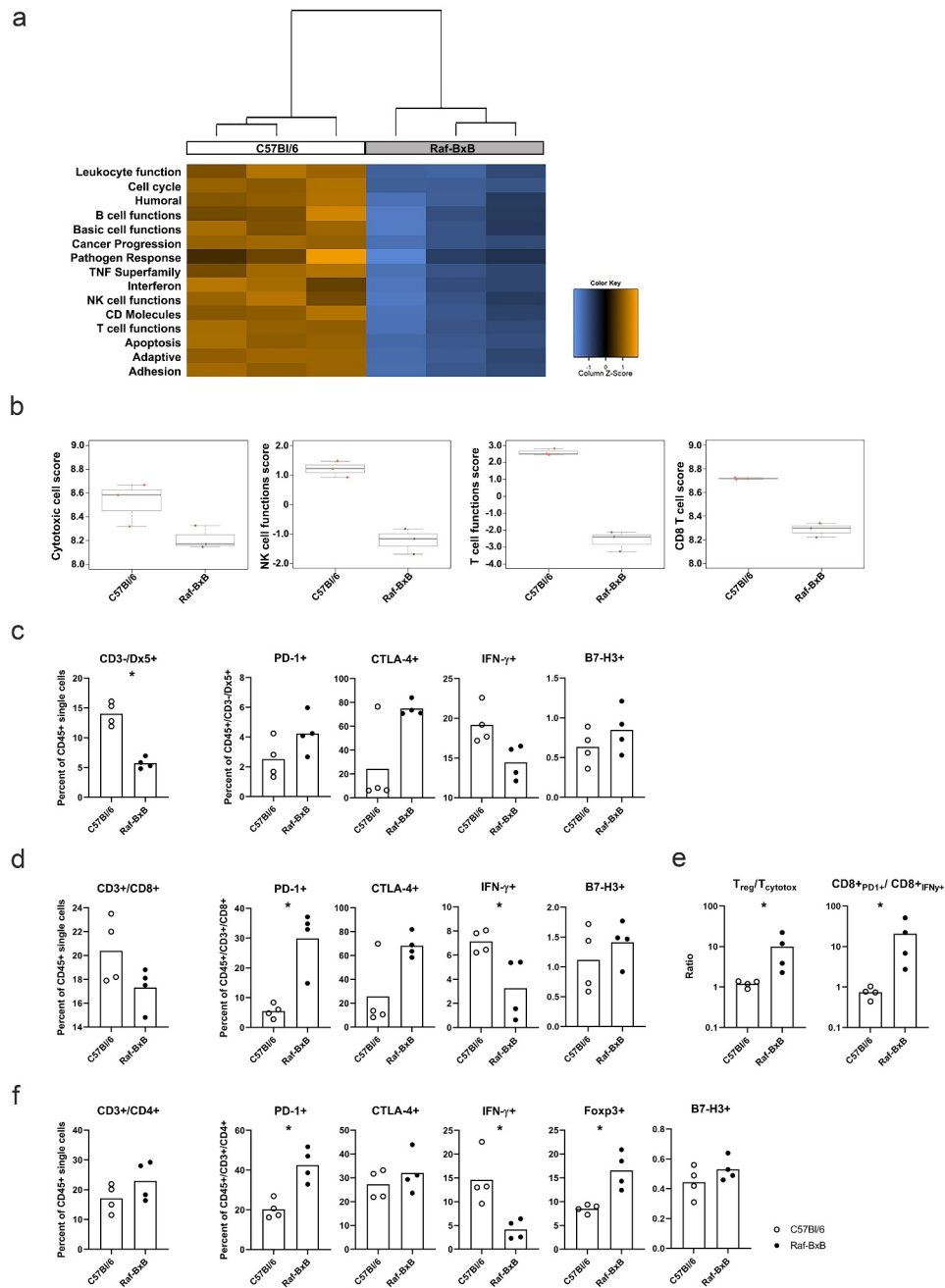
Figure 2. Progressive NSCLC growth affects lung infiltration and activation of NK and T lymphocyte subsets in the lungs of Raf-BxB mice. (A-B) Total lung RNA of C57Bl/6 WT or NSCLC-bearing Raf-BxB mice of the same age was isolated and multiplex gene expression analysis was performed with the nCounter® PanCancer Immune Profiling Panel and subsequent analysis with the nSolver analysis software. (A) Heatmaps represent data of the 15 most substantially downregulated functional cancer or immunology-related cluster in the lungs of Raf-BxB mice compared to WT mice. Heatmaps of three individual animals per group are shown. (B) Functional and relative scores of selected immune cell subsets determined via nSolver advanced analysis are indicated. (C-E) Lungs of C57Bl/6 WT and Raf-BxB mice were enzymatically processed and single lung-derived living CD45$^+$ immune cells were investigated for levels of NK cells (CD3$^-$/Dx5$^+$) (C), cytotoxic T lymphocytes (CD3$^+$/CD8$^+$) (D) and T helper cells (CD3$^+$/CD4$^+$) (F) (left panels) and percentages of the respective subsets positive for the indicated intra- and extracellular activation markers (C, D, F, right panels) were determined by multi-color flow cytometry. (E), Ratios of regulatory T cells (T$_{reg}$) (CD3$^+$/CD4$^+$/Foxp3$^+$) to activated cytotoxic T lymphocytes (T$_{cytotox}$) (CD3$^+$/CD8$^+$/IFNγ^+) (left graph) and PD1$^+$/CD8$^+$ (CD8+ $_{PD1+}$) to IFNγ^+/CD8$^+$ (CD8+ $_{IFN\gamma+}$) T lymphocytes (right graph) are shown. The detailed gating strategy is presented in Supplementary Figure 2.

resulting in immune cell suppression and immune evasion of NSCLCs.

Combination of oncolytic IAV and PD-1 ICI does neither increase oncolytic efficacy nor extend immune cell activation against NSCLCs in vivo

To test whether virus-mediated cancer cell lysis might be improved by combined treatment with oncolytic IAV and PD-1 IC inhibitor, Raf-BxB mice were intranasally infected with a sublethal dose of influenza A virus PR8 and additionally subjected to a therapy with α-PD-1 monoclonal antibodies (mAbs).
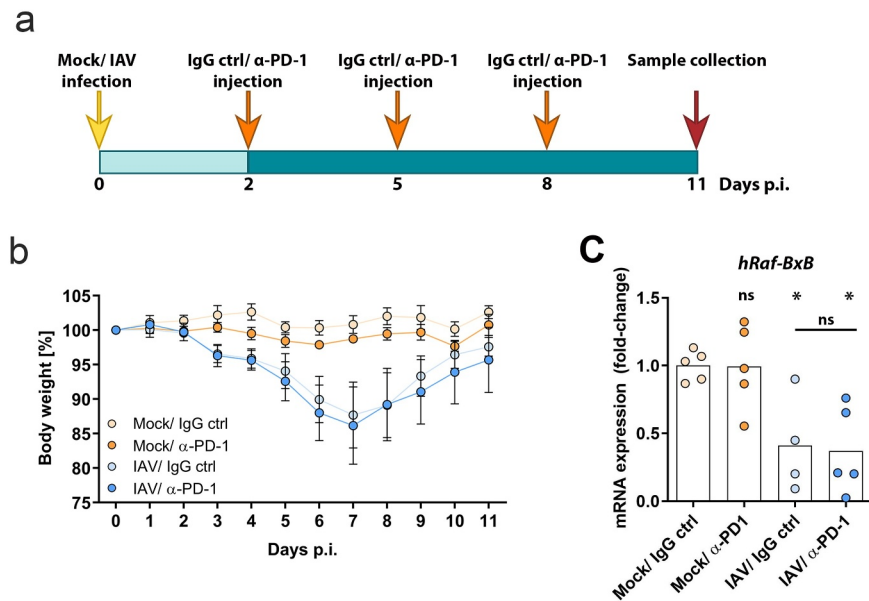
Figure 3. Combination of oncolytic IAV and α-PD-1 ICIs does not increase therapeutic activity mediated by IAV infection. Raf-BxB mice were intranasally infected with a sublethal dose of 500 pfu of IAV (A/Puerto Rico/8/1934) per mouse or solvent control (mock). Two days post infection mice were intraperitoneally injected, each third day, with 250 μg of α-PD-1 monoclonal antibodies or 250 μg of the respective isotype control (IgG ctrl). (A) Schematic representation of the experimental approach. (B) Bodyweight loss of the treated mice representing disease onset was investigated daily. Mean values of 5 mice per group ±SEM are depicted. (C) Eleven days post infection total RNA was isolated from lung lysates and mRNA expression levels of oncogenic Raf-BxB was investigated via RT-qPCR. Values were normalized to mRNA expression levels of the housekeeping genes GAPDH and Cytochrome C and the mean value of control Mock/IgG ctrl mice was arbitrarily set to 1. n-fold mRNA expression levels are presented.

The ICI was injected intraperitoneally every third day beginning 2 days after infection (Figure 3a, IAV/α-PD-1) and the oncolytic efficacy was investigated 11 days post infection. Three control groups of Raf-BxB mice were analyzed. The first group received mock-infection and control IgG antibodies only (Mock/IgG ctrl). The other two groups were either mock-infected with the virus-solvent control but received specific α-PD-1 antibodies (Mock/α-PD-1) or were infected with IAV but treated with control IgG (IAV/IgG ctrl). The experimental setup is based on studies by Rojas *et al.*, who described that tumor cell lysis and TAA release should precede ICI application to achieve best immunotherapeutic efficacy.[22]

The efficiency of viral infection and the health status of the treated mice were monitored by following body weight (Figure 3b). As expected, IAV-infected groups start to lose weight from day 2 post infection. The bodyweight decline lasted until day 7, after which it began to recover and at day 11 of infection the mice recovered their initial bodyweight. Mock-infected control mice did neither lose bodyweight nor show any signs of disease, independently of treatment with α-PD-1 or respective IgG control antibodies.

The oncolytic efficacy was assessed by measuring mRNA levels of oncogenic *Raf-BxB* in total lung RNA lysates by day 11 post infection (Figure 3c). As demonstrated earlier, mRNA levels correlate with lung-tumor mass and could thus be taken as a measure to represent therapeutic efficacy.[19] Treatment of Raf-BxB mice with α-PD-1 monoclonal antibodies only did not change mRNA expression levels in the lungs of Raf-BxB mice compared to the untreated controls, indicating that PD-1 blockade alone does not provide therapeutic activity. To the contrary, IAV infection alone resulted, as expected, in a significant reduction of oncogenic Raf expression of about 55%. Surprisingly,

combined treatment of Raf-BxB mice with oncolytic IAV and PD-1 ICI did not lead to significant increase of cancer cell lysis. Thus, combining oncolytic IAV infection with PD-1 ICI did not improve the therapeutic efficacy.

Along that line, application of the α-PD-1 ICI alone or in combination with IAV infection unveiled no additional recruitment or activation of lung-derived alveolar (CD45$^+$/F4/80$^+$/CD11b$^-$/CD11c^{hi}/SigF$^+$) or peripheral (pMφ; CD45$^+$/CD11b$^+$/F4/80$^+$/SigF$^-$/CD11c$^-$) macrophages, as well as NK cells (CD45$^+$/CD3$^-$/Dx5$^+$) or T lymphocyte subsets (CD45$^+$/CD3$^+$/CD4$^+$ T helper cells; CD45$^+$/CD3$^+$/CD8$^+$ cytotoxic T cells) compared to the respective mock- or IAV-infected IgG controls (Supplementary Figure 1). The binding efficacy of the α-PD-1 IC antibody to lung-derived T lymphocytes in treated mice was verified by flow cytometry. The percentage of T helper cells able to bind the α-PD-1 antibody was significantly lower in lungs of IAV/α-PD-1-treated mice than in IAV/IgG ctrl- or IAV/α-B7-H3-treated control mice, most probably due to efficient binding of the applied IC antibodies to lung T helper cells, as the same antibody clone that was injected into mice was used for flow cytometry T cell staining (Supplementary Figure 1i).

Overall, these data indicate minor involvement of PD-1-mediated immune-checkpoint signaling in the lungs of Raf-BxB mice, even though the receptor is highly overexpressed on lung-derived NK and T lymphocyte subsets.

Combination of oncolytic IAV and B7-H3 immune checkpoint inhibitor results in superior therapeutic efficacy against NSCLCs in vivo

Recent studies of patient-derived NSCLC tissues demonstrated an overexpression of B7-H3 in 70–80% of cases, which correlated critically with CD8$^+$ T cell suppression and

nonresponsiveness to α-PD1 therapy.[23] As application of PD-1 ICI did not improve IAV-mediated oncolytic and immunostimulatory properties, we aimed to examine the combination of B7-H3 ICI and oncolytic IAV treatment. As for IAV and PD-1 combinational application, Raf-BxB mice were intranasally infected with IAV virus (IAV) or solvent control (mock) with following injection of α-B7-H3 mAbs (α-B7-H3) or the respective IgG control (IgG ctrl). The antibodies were injected i.p. every third day beginning from day two of infection (Figure 4a) and the therapeutic efficacy was investigated 11 days post infection. As already observed upon α-PD-1 treatment, mice injected with α-B7-H3 antibody only did not lose any bodyweight (Figure 4b). In comparison, IAV infection resulted in bodyweight loss and acute infection onset, as expected. Interestingly, combined treatment with oncolytic IAV and α-B7-H3 antibodies resulted in a transient bodyweight loss during acute infection, reaching a maximum weight loss at day 7 post infection. However, all mice completely recovered and gained bodyweight until day 11 post infection and did not show remaining disease symptoms.

While application of α-B7-H3 monoclonal antibodies alone did not alter oncogenic Raf-BxB mRNA levels, IAV infection *per se* resulted in significant reduction of their expression by 53% (Figure 4c). Strikingly, the combined application of oncolytic IAV and B7-H3 ICI led to a further significant improvement of the therapeutic efficacy as evidenced by the reduction in oncogenic Raf-BxB mRNA expression of 81% in comparison with untreated (Mock/IgG ctrl) control mice.

Efficient application of ICIs to tumor-bearing mice shall generally interfere with cancer-mediated immunosuppression and, thus, improve the overall immune responses. Hence, viral replication could be influenced by ICI application, which should not happen in case of IAV infection with IgG controls. To exclude that the observed oncolytic effect was based on differences in viral replication, lung virus titers were evaluated at day 5 of infection, e. g. 3 days after the first ICI application. As evidenced by standard plaque assay, α-B7-H3 mAb application did not affect viral replication in the lungs of NSCLC-bearing Raf-BxB mice compared to the respective IgG control infected mice (Figure 4d).

Thus, despite comparable virus replication, combined application of oncolytic IAV and α-B7H3 antibodies resulted in a remarkably improved oncolysis that was superior to single IAV infection.

Combination of oncolytic IAV and B7-H3 immune checkpoint inhibitor results in upregulation of surface MHCII on alveolar macrophages and recruitment of activated NK cells and CD8^{+} T lymphocytes into the lungs of Raf-BxB mice

Because the enhanced therapeutic effect in B7-H3-treated IAV-infected mice was not accompanied by altered viral replication, we hypothesized that the enhanced therapeutic effect is more likely a consequence of the increased lung recruitment and activation of immune cells. Thus, we aimed to investigate differential recruitment and activation of cytotoxic innate and adaptive immune cell subsets to the lungs upon treatment.

Single application of B7-H3 ICI unveiled no immunomodulatory properties, affecting neither alveolar (aMφ) or peripheral (pMφ) macrophage subsets nor NK or T lymphocyte recruitment or activation, indicating that B7-H3 blockade alone is not sufficient to overcome the NSCLCmediated immune-evasion mechanisms (Figure 5). IAV infection alone also did not significantly affect the absolute numbers of alveolar macrophages (CD45^{+}/F4/80^{+}/CD11b/CD11c^{hi}/Siglec-F^{+}) (aMφ) in the lungs of infected mice (Figure 5a). However, after dual treatment with IAV and B7-H3 ICI, their maturation was significantly increased compared with mice treated with a single agent, as indicated by increased geometric mean fluorescence intensity (GeoMFI) of MHCII (Figure 5b). Compared
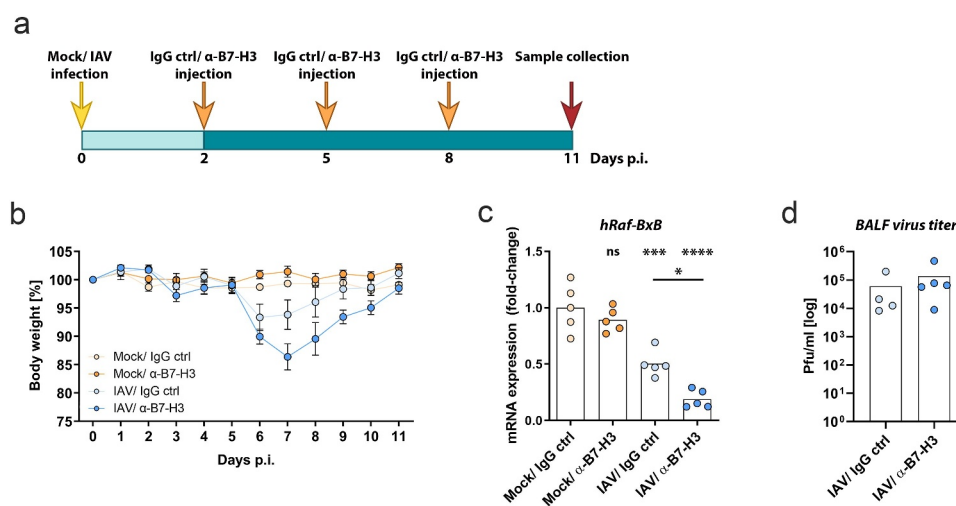

Figure 4. Combination of oncolytic IAV and B7-H3 ICI synergistically promotes NSCLC oncolysis. Raf-BxB mice were intranasally infected with a sublethal dose of 500 pfu of IAV (A/Puerto Rico/8/1934) per mouse or solvent control (mock). Beginning from day two of infection, mice were intraperitoneally injected each third day with 250 µg of α-B7-H3 monoclonal antibodies or 250 µg of the respective isotype control (IgG ctrl). (A) Experimental approach schedule. (B) Bodyweight loss of the treated mice representing disease onset was investigated daily. Mean values of 5 mice per group ±SEM are depicted. (C) Eleven days post infection RNA was isolated from total lung lysates and mRNA expression levels of oncogenic Raf-BxB representing lung cancer burden was investigated via RT-qPCR. Values were first normalized to mRNA expression levels of the housekeeping genes GAPDH and Cytochrome C and the mean value of control Mock/IgG ctrl mice was arbitrarily set to 1. n-fold mRNA expression levels are presented. (D) Virus titers presented as pfu/ml were determined in BAL samples 5 days post infection by standard plaque assay
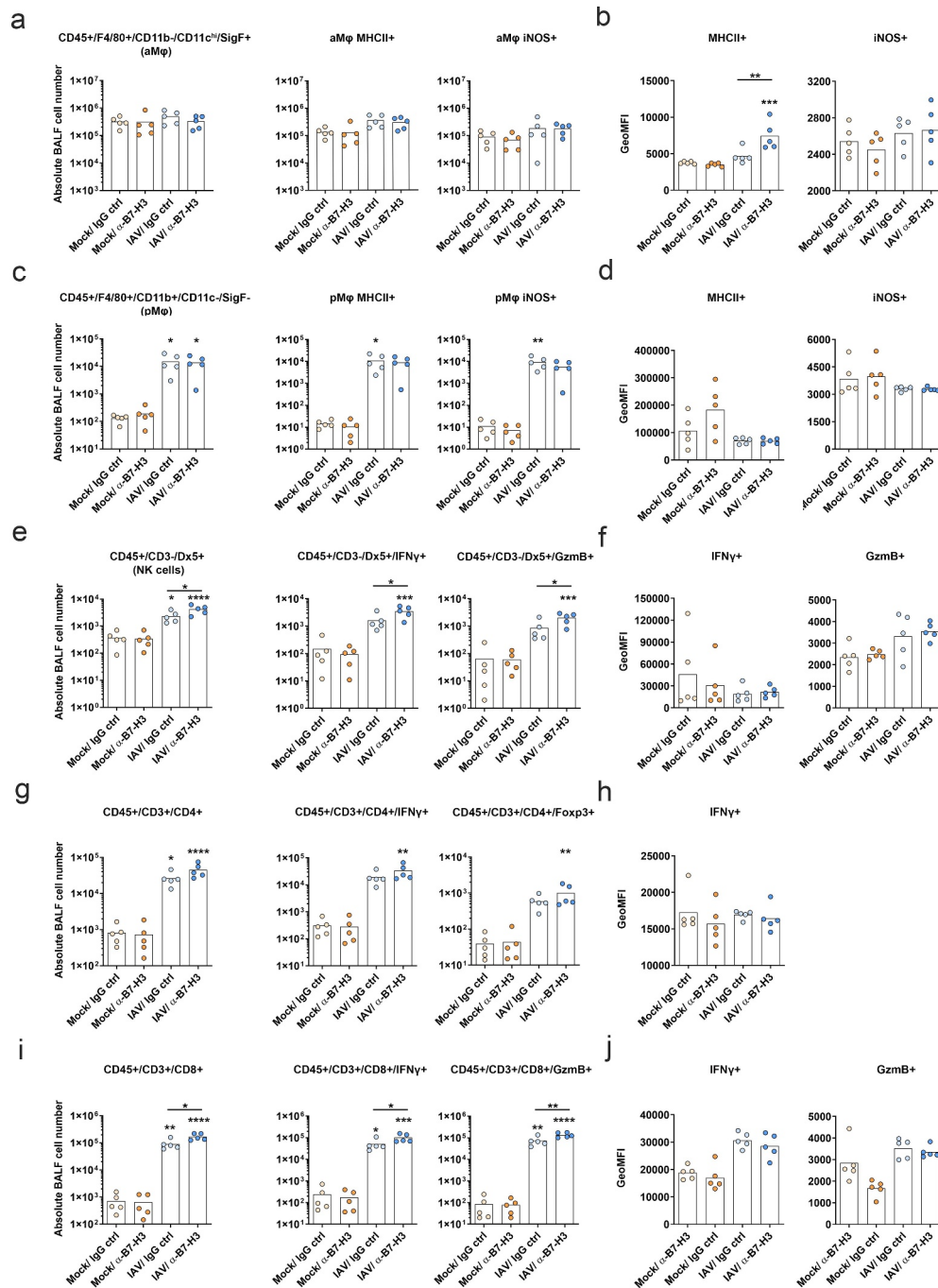
Figure 5. Combined application of oncolytic IAV and B7-H3 ICI results in increased lung recruitment of activated NK cells and cytotoxic T lymphocytes. Raf-BxB mice were intranasally infected with IAV or solvent control (Mock) and received injections of monoclonal α-B7-H3 antibodies or the respective IgG ctrl as indicated in Figure 4A. Eleven days post infection, BALF-derived immune cells were analyzed for immune cell subsets and their respective activation markers by multi-color flow cytometry. Absolute single cell numbers of overall BALF-derived alveolar macrophages (CD45$^+$/F4/80$^+$/CD11b$^-$/CD11c^{hi}/SiglecF$^+$)(aMφ) (A, left panel), peripheral macrophages (CD45$^+$/CD11b$^+$/F4/80$^+$/CD11c$^-$/SigF$^-$) (pMφ) (C, left panel), NK cells (CD45$^+$/CD3-/Dx5$^+$) (E, left panel), CD4 + T cells (CD45$^+$/CD3$^+$/CD4$^+$) (G, left panel) and CD8 + T cells (CD45$^+$/CD3$^+$/CD8$^+$) (I, left panel) are presented. (A, C, E, G and I right panels) Absolute numbers of the respective immune cell subsets positive for the indicated intra- and extracellular markers are represented. (B, D, F, H and J) GeoMFI of the respective immune cell subsets positively gated for the indicated marker proteins are presented. The detailed gating strategy is presented in Supplementary Figure 3 and representative dot plots for one mouse per group including FMO controls are shown for each activation marker in Supplementary Figure 4.

to aMφ, IAV infection resulted in increased recruitment of activated peripheral macrophages (CD45$^+$/CD11b$^+$/F4/80$^+$/SigF/CD11c$^-$) (pMφ) (Figure 5c). In contrast, the total number of activated peripheral macrophages or their activation level did not differ between IAV infection alone and double treatment with IAV and B7-H3 ICI (Figure 5c, d), indicating

a minor role of these immune cells in enhanced therapeutic efficacy after combined application. In comparison, the recruitment of activated IFNγ$^+$ and GzmB$^+$ NK cells was significantly increased in the BALFs of double-treated mice

(Figure 5e), while levels of IFNγ or Granzyme B (GzmB) per NK cell did not significantly differ (Figure 5f).

As expected, IAV infection alone provoked a significant increase in lung infiltration by activated T helper cells (CD45^{+}/CD3^{+}/CD4^{+}) (Figure 5g). While the number of activated T helper cells, indicated by IFN-γ+ cells, was increased after IAV infection, combined treatment only tended to but did not significantly increase the cell numbers of activated T-helper cells in the lungs. In accordance, levels of IFNγ-expression per cell were not altered (Figure 5h). Similarly, the numbers of Tregs did not differ in double treated and IAV-infected mice. These data imply a rather minor role of combined treatment on T helper and regulatory T cells in improved cancer cell killing.

Most remarkably, IAV infection also resulted in increased lung recruitment of cytotoxic T lymphocytes (CD45^{+}/CD3^{+}/CD8^{+}) (Figure 5i).Interestingly, in contrast to single application of IAV or B7-H7 ICI, their combination resulted in significantly increased recruitment and activation of these immune cell subsets. Most evidently, combined application of oncolytic IAV and B7-H3 ICI increased lung recruitment of activated IFNγ+ and GzmB+ cytotoxic T lymphocytes (Figure 5j).

In summary, single application of α-B7-H3 antibodies did not alter immune cell recruitment or activation, while IAV infection per se resulted in increased immune cell recruitment and activation. Finally, the combined application of oncolytic IAV and B7-H3 ICI further enhanced alveolar macrophage activation (corresponding to increased expression of MHCII) and further significantly increased lung infiltration by activated NK cells and cytotoxic T lymphocytes. Increased cancer cell lysis and higher T lymphocyte infiltration was further confirmed by comparative immunohistochemistry staining of paraffin-embedded lung lobes (Figure 6). Consistent with Raf-BxB oncogene mRNA expression levels (Figure 4c), injection of α-B7-H3 antibodies alone did not induce tumor shrinking, while IAV infection resulted in considerable tumor shrinking (Figure 6a, b). Strikingly, combined IAV and ICI treatment exhibited a higher lung inflammation but also a substantially increased reduction of overall tumor foci number and size 11 days post infection.

Flow cytometry analyses revealed remarkably increased lung infiltration of cytotoxic T lymphocytes (Figure 5i) in double-treated mice compared to the other groups. These data were confirmed by CD3 staining of respective lung lobes in immunohistochemistry (Figure 6c). Most strikingly, lung section areas infiltrated with CD3^{+} T lymphocytes appeared to be almost completely cleared of cancer foci. Indeed, the disintegration of distinct tumor foci was improved upon double treatment compared to IAV infection alone. In contrast, the level of tumor-infiltrating T lymphocytes was low in non-infected mice, demonstrating a rather low overall T lymphocyte lung-infiltration. Single application of B7-H3 ICI did not improve T cell recruitment to tumor site.

Infection with oncolytic IAV leads to transient upregulation of PD-L1 and PD-L2 but maintained upregulation of B7-H3 in the lungs of Raf-BxB mice

Recent studies demonstrated that unresponsiveness of tumor patients to PD-1/PD-L1 IC therapy was associated to overexpression of B7-H3 or to mutations of the tumor-associated EGFR.[23–25]

In addition, the expression of PD-L1 has been demonstrated to be related with the efficacy of PD-1/PD-L1 blockade therapy in NSCLC.[26] Furthermore, it was shown that infection with OV promotes up-regulation of PD-L1 in the tumor microenvironment via interferon signaling, thereby increasing the sensitivity to PD-1 therapy of resistant cancers.[27,28]

To gain a mechanistic insight into oncolytic IAV-mediated checkpoint expression during acute virus infection, C57Bl/6 WT and tumor-bearing mice were infected with IAV and changes in IC ligand expression was analyzed by qRT-PCR (Figure 7). As virus replication differs significantly in C57Bl/6 and Raf-BxB mice,[19] the infectious dose was adjusted to comparable sublethal doses. In both, C57Bl/6 (Figure 7a) and Raf-BxB mice (Figure 7b), IAV infection resulted in significant transient upregulation of *PD-L1* and *PD-L2*. The expression levels reached a peak at day 6 post infection and declined again at day 12 post infection. Of note, mRNA expression of PD-L1 and PD-L2 no longer showed significant differences from uninfected mice at day 12 post infection. As expected, the expression pattern correlated with IFNγ gene expression levels.

Significant upregulation of *B7-H3* upon IAV infection was also observed in C57Bl/6 WT mice. However, in comparison to *PD-L1* and *PD-L2, B7-H3* was continuously upregulated to significantly increased levels on day 6 and 12 post infection and did not decline during the whole observation time. Remarkably, Raf-BxB mice already showed a 4-fold higher expression level of B7-H3 in lung lysates from uninfected mice compared with WT mice (see Figure 1). Interestingly, even though lung cancer tissue was significantly decreased upon oncolytic IAV infection (see Figures 3, 4 and 6), expression levels of *B7-H3* remained constantly high in the lungs of IAV-infected tumor-bearing Raf-BxB mice. Given that NSCLC cells express high levels of B7H3 and that IAV infection generally leads to upregulation of B7-H3, these data imply an equalization of overall *B7-H3* expression levels due to its decrease because of cancer cell destruction and the upregulation mediated by IAV infection.

In summary, PD-L1 and PD-L2 expression is transiently upregulated in both WT and tumor-bearing mice, correlating with IFNγ levels. In contrast, B7-H3 showed a prolonged upregulation pattern that reached a maximum at later time points after infection in WT mice. However, in the lungs of Raf-BxB mice, B7-H3 expression is constitutively high and remained at consistently high levels even after oncolytic IAV infection.

Discussion

In this study, we utilized a fully immunocompetent syngeneic murine model for slowly growing lung cancers, closely representing the clinical phenotype and immunosuppressive characteristics of human NSCLCs. We outlined overexpression of the IC ligand B7-H3 by NSCLC cells as well as by immunosuppressive lung-resident alveolar macrophages.[19] In agreement with this, we identified exhausted NK- and T cell subsets overexpressing the IC receptor PD-1 and producing reduced amounts of pro-inflammatory mediators such as IFN-γ in lungs of NSCLCbearing mice. Finally, we demonstrated that inhibition of PD-1 or B7-H3 ICs alone is rather ineffective against NSCLCs, but
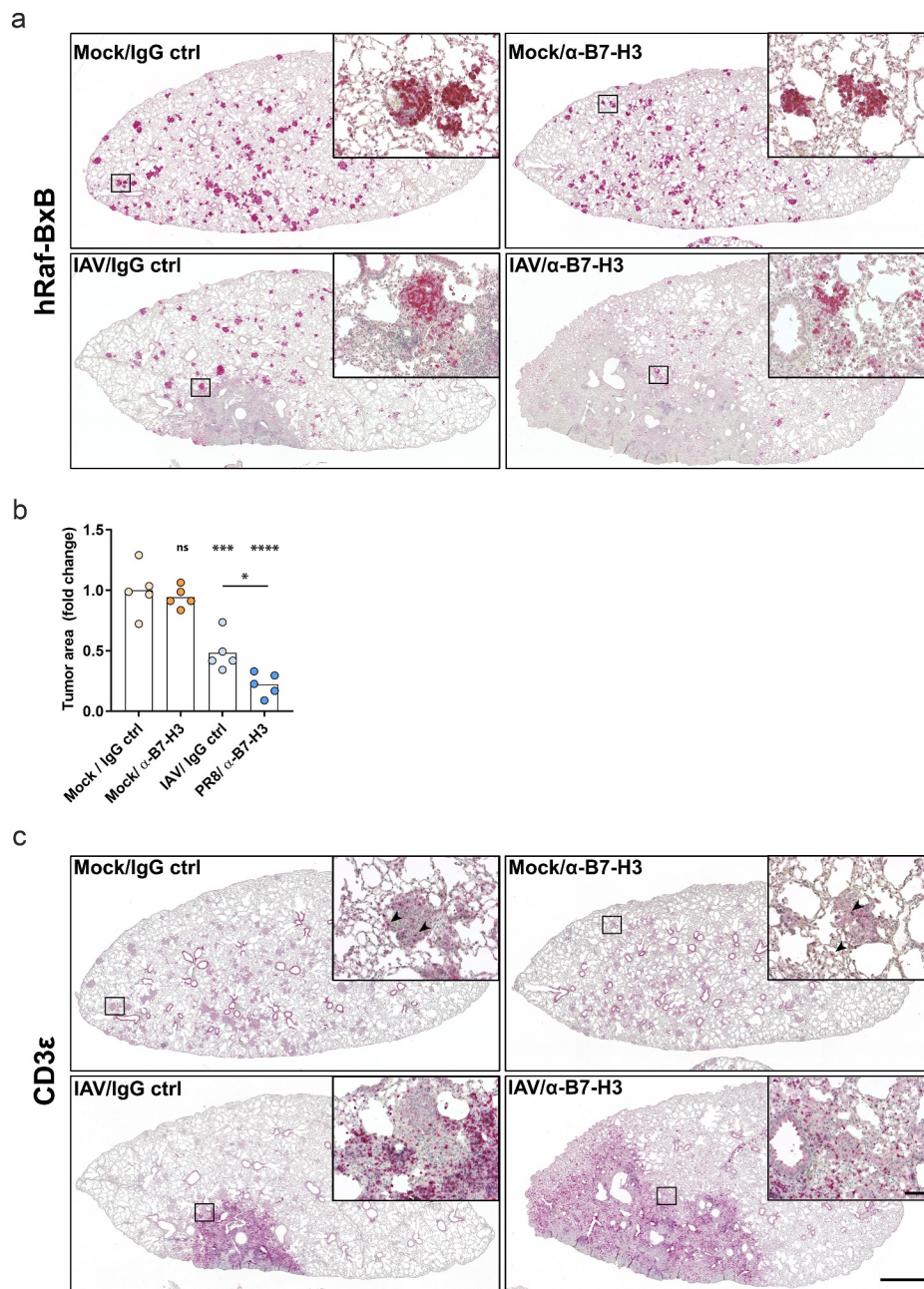
Figure 6. Combination of oncolytic IAV infection and B7-H3 ICI application leads to tumor foci destruction and increased lung- and tumor-infiltration with T lymphocytes. Raf-BxB mice were intranasally infected with IAV or solvent control (Mock) and received injections of monoclonal α-B7-H3 antibodies or the respective IgG ctrl as indicated in Figure 4A. Sequential paraffin lung tissue sections were stained for human Raf-BxB representing oncogene expressing tumor foci (A) or CD3ε⁺ indicating T lymphocyte lung infiltration (B) and counterstained with hematoxylin. Merge pictures of one lung lobe and respective detail pictures of higher magnification of one representative mouse per group are shown. Bars represent 1000 μm (merge pictures) or 100 μm (close up pictures). (C) For absolute quantification of tumor tissue area, three different sections of each mouse lung stained by IHC for hRAf-BxB were quantified from 5 mice per group. The area of the hRAf-BxB-positive tumor foci was quantified and expressed in relation to the total section area of each lung lobe. Means of three quantified layers per mouse are indicate as one individual entry. n-fold tumor area normalized to the control group (Mock/IgG ctrl) are presented.

combined with oncolytic IAV infection, inhibition of B7-H3, but not of PD-1, was extremely efficient in tumor cell destruction, reducing their amount up to 80%. These data are in line with and further extend the clinical findings demonstrating the overexpression of these checkpoint molecules on cancer cells and TAMs derived from NSCLC patients.[29–31] To our knowledge, we are the first to present an additive therapeutic effect of oncolytic viruses and B7-H3 ICI therapy against NSCLCs. Thus, additional future studies are needed to verify superior therapeutic efficacy in further preclinical models of primary lung cancer.

Application of mAbs against the PD-L1/PD-1 immune-checkpoint pathway was already approved as standard of care treatment for NSCLCs with impressive response rates in some cases. However, in most patients the effect fell short of expectations.[2] Our data closely resemble these results, as IC blockade of PD-1 did neither result in cancer rejection (Figure 3) nor in overall immune cell activation or cytotoxic NK and T-cell recruitment *in vivo* (Supplementary Figure 1). Notwithstanding, PD-1 was significantly upregulated on NK and T lymphocyte subsets in murine lungs with NSCLCs and PDL-2 as the respective
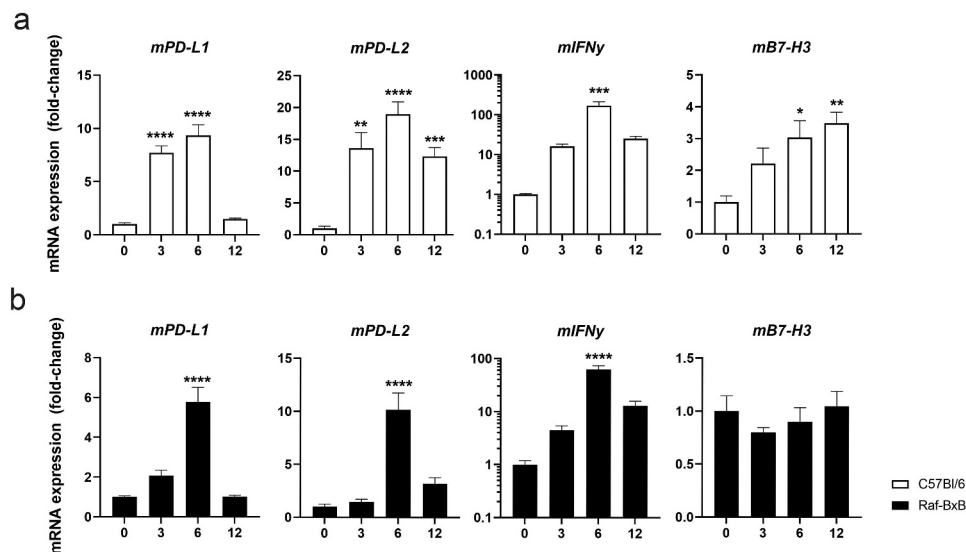
Figure 7. Infection with oncolytic IAV leads to transient upregulation of PD-L1 and PD-L2 but prolonged upregulation of B7-H3 in the lungs of C57Bl/6 and Raf-BxB mice. C57Bl/6 WT (white bars) or NSCLC-bearing Raf-BxB mice (black bars) were intranasally infected with sublethal doses of 300 pfu (WT) or 500 pfu (Raf-BxB). At the indicated time points total lung lysates were investigated for mRNA expression levels of immune checkpoint molecules via TaqMan RT-qPCR. The values were first normalized to mRNA amounts of the housekeeping genes GAPDH and Cytochrome C and the mean value of WT mice was arbitrarily set to 1 and fold-change mRNA expression levels are presented. Mean values ± SEM of 4–6 animals per group are presented.

suppressive ligand was found to be overexpressed on a fraction of lung-derived TAMs. However, the overall PD-L1 expression was downregulated, seemingly not being relevant for immune evasion in the lungs of Raf-BxB mice.

B7-H3, a newly described immune-checkpoint ligand, was demonstrated to be overexpressed in the majority (70–80%) of lung tissues derived from NSCLC-patients.[32] Its overexpression rate in NSCLC patient samples is more frequent than the previously described IC ligands such as PD-L1. Furthermore, overexpression of B7-H3 in patients correlated with unresponsiveness to PD-1 ICI therapy and poorer overall survival.[23] Our findings are in well accordance with these results, as B7-H3 IC ligand was substantially upregulated in both cancer cells and tumor-associated alveolar macrophages, implying a dual blockade of T cell function. However, our data showed that suppression of neither PD-1 nor B7-H3 IC results in cancer cell rejection (Figure 3, 4, 6) or immune cell recruitment and activation (Figure 5, Supplementary Figure 1). These data underline that ICI application might be insufficient for established solid cancers, even though the respective molecules are overexpressed and appear as attractive therapeutic targets. This assumption is supported by the fact that the overall level of effector T lymphocyte lung infiltration in Raf-BxB mice was low, independently of IgG ctrl or specific ICI application (Supplementary Figure 1, Figure 5, Figure 6 arrows). However, the applied ICIs were not potent enough to overcome the diversity of immunosuppressive properties of NSCLCs in the lungs of immunocompetent Raf-BxB mice.

The role of TAMs in ICI-resistance of NSCLCs is vitally important, as they are the most abundant tumor-infiltrating immune cell type. They function as a transition point not only being suppressed by cancer cells, but also act in concert with cancer cells to suppress other immune cell subsets. Recent studies highlighted a critical role of TAMs in the resistance to therapeutic immune responses, due to expression of immune-checkpoint molecules such as PD-L1,[33,34] PD-L2[35] or B7-H3[4], which suppresses recruitment, in situ proliferation and cytotoxic cellular immune responses of NK or T cells.[36] Thus, polarization of TAMs to an M1-like phenotype is key to improve efficacy of ICI therapy, as activated macrophages mount robust anti-tumoral responses and are able to directly kill cancer cells. In addition they support adaptive immune responses by presenting tumor-associated antigens and production of chemokines and cytokines that recruit and activate cytotoxic immune responses.[37] Thus, several immunomodulatory agents were suggested to be combined with ICI therapies, including oncolytic viruses. The oncolytic potential of influenza A virus infection of cancer cells is described by several groups in *in vitro* and *in vivo* preclinical studies.[12,38–40] Since our previously published studies were performed in a fully immunocompetent mouse model, we could additionally demonstrate impressive immunomodulatory potential of endotracheal applied IAV *in vivo* resulting in alveolar TAM-repolarization to a pro-inflammatory active phenotype comprising immune cell-mediated cytotoxicity.[19] Even though polarized TAMs demonstrated pro-inflammatory properties, they did not reach activation levels of alveolar macrophages of infected WT mice.[19]

To improve IAV-induced oncolytic properties and increase M1-like properties of alveolar TAMs as well as recruitment and activation of cytotoxic effector cells by IAV infection, we combined IAV infection with either PD-1 or B7-H3 ICIs. Combination of IAV with B7-H3 ICI significantly improved the outcome of cancer cell lysis and ameliorated the IAV-mediated immunomodulation, demonstrated by enhanced levels of MHCII surface presentation on alveolar macrophages and increased cytotoxic NK and T-cell recruitment.

Although the overall standard deviation was slightly higher in the group treated with PD-1 ICI and IAV than in the group treated with B7-H3 ICI and IAV, we can conclude that the

combination of IAV and PD-1 ICI did not significantly improve therapeutic efficacy or recruitment or activation of immune cells. To interpret the failure of combined anti-PD-1 and oncolytic IAV treatment, the individual expression pattern of PD-L1 and PD-L2 have to be considered. Although PD-1 was overexpressed on lung infiltrating T lymphocytes (Figure 2), the PD-1 binding ligands, PD-L1 and PD-L2, exhibited an inverse expression pattern. Because the overall lung *PD-L1* expression was significantly reduced in Raf-BxB compared with WT mice and the *PD-L2* expression was unaltered (Figure 1), it appears unlikely that NSCLC cells in the lungs of Raf-BxB mice overexpressed these ligands. Nevertheless, significantly more albeit overall low levels of TAMs exposed PD-L2 on their surface. Overall, the PD-L2/PD-1 immune-checkpoint signaling is presumably not the major immune-evasion mechanism of RafBxB NSCLCs, as PD-1 ICI did not improve the overall therapeutic outcome.

Interestingly, as previously shown for other OVs,[27,28] infection with oncolytic IAV resulted in transient and significantly increased expression of *PD-L1* and *PD-L2* during acute infection (see Figure 7). This could presumably increase the sensitivity to PD-1 checkpoint therapy.[27,28] However, by day 12 post infection, the expression of both, PD-L1 and PD-L2, was again decreased and their levels were comparable to those found in uninfected lungs. Interestingly, surface expression of the inhibitory receptor PD-1 on T lymphocyte subsets was increased in the lungs of Raf-BxB mice (Figure 2). In this context, we have recently demonstrated that oncolytic IAV infection also leads to upregulation of PD-1 on both, CD4$^+$ and CD8$^+$ lung T lymphocytes, reaching a peak on day 9 post infection in of WT mice and declining again on day 12 after infection.[11]

Taken together, these data suggest a transient potentiation of PD-L1 and PD-L2 expression by IAV infection. However, this transiently increased sensitivity to PD-1 therapy does not appear to be durable enough to increase T lymphocyte activity at later stages after infection, when the adaptive immune response is expected to exert its anticancer effects.

Conversely, we demonstrated substantial overexpression of the immune-checkpoint ligand B7H3 by cancer cells (Figure 1a, b) and increased levels of alveolar TAMs (Figure 1e) in NSCLC-bearing mice. In comparison, B7H3 was neither expressed on NK cells nor T lymphocyte subsets (Figure 2c, d, f). These data suggest a more pronounced bipartite role of B7H3 in the immune evasion of NSCLCs. Though the respective inhibitory receptor for B7H3 is still not identified, inhibitory action of B7H3 toward NK cell function as well as Tlymphocyte proliferation and activation was demonstrated by several studies.[4,5,41] However, recent investigations propose an additional immunosuppressive role of B7H3 on macrophage differentiation to a TAM phenotype via a putative B7H3 receptor on macrophages.[42,43] These data imply a complex dual inhibitory function of B7H3, not only affecting cytotoxic T lymphocyte function, but also macrophage activation and polarization. These macrophages in turn, affect T lymphocyte cytotoxic functions, resulting in a multileveled immunosuppression.[42] These findings might explain increased alveolar macrophage MHCII surface presentation upon combined oncolytic IAV infection and α-B7-H3 antibody application (Figure 5a) and hence the increased lung infiltration by cytotoxic NK cells and T lymphocytes (Figure 5f), which finally resulted in elevated cancer cell lysis. Accordingly, immunohistochemistry staining of lung sections for CD3$^+$ T lymphocytes (Figure 6) highlighted increased tumor infiltration with T lymphocytes upon double treatment. While IAV infection alone already resulted in T lymphocyte recruitment and cancer cell lysis in highly CD3$^+$ T cell infiltrated areas, recruitment of T lymphocytes was limited, and tumor-infiltration was only partial. Presumably, because B7H3 expressing cancer cells and TAMs in the TME dampen tumor infiltration to a certain extend.

In contrast, double treatment with IAV and α-B7-H3 antibody resulted in substantial CD3$^+$ T lymphocyte tumor infiltration and more pronounced cancer foci destruction. Considering that oncolytic IAV infection itself promotes prolonged B7-H3 expression in the lungs of WT mice (Figure 7), this highlights the particular importance of B7-H3 blockade at different stages during combined NSCLC immunotherapy.

In conclusion, using a pre-clinical fully immunocompetent *in vivo* model for NSCLCs, we have demonstrated synergistic oncolytic and immunomodulatory action of combined oncolytic IAV infection and B7-H3 ICI for lung cancers, resistant to single ICI-treatment. Thus, individualized therapy with synergistically acting oncolytic viruses and B7-H3 ICIs might be an innovative approach to overcome immune-evasion mechanisms in NSCLC patients' resistant to established ICIs and may improve the therapy outcome in the future.

Material and methods

Ethics statement

All animal studies were performed in accordance with the German regulations of the Society for Laboratory Animal Science (GVSOLAS) and the European Health Law of the Federation of Laboratory Animal Science Associations (FELASA). The protocols were approved by the Landesamt für Natur, Umwelt und Verbraucherschutz Nordrhein-Westfalen (LANUV-NRW), Germany.

Animal experiments

All experiments were performed with 4–8 month-old homozygous transgenic *c-Raf-1-BxB* (*RafBxB*)[18] or C57Bl/6 (WT) mice of both genders that were kept under pathogen-free conditions. For IAV infection, a total volume of 50 μl of viral inoculum was intranasally administered. Administration of PBS alone (mock) served as a control. All infection experiments were performed with a sublethal dose of 500 plaque-forming units (pfu) for Raf-BxB mice or 300 pfu for C57Bl/6 mice of the influenza virus strain A/Puerto Rico/8/34 (PR8, H1N1) as described earlier.[11,19] The number of infectious virus particles in the bronchoalveolar fluid (BALF) was determined by standard plaque assay as previously described[44] and viral titers were expressed as plaque-forming units (pfu) per ml.

For immune-checkpoint treatment, mice were receiving i.p. injections of 250 μg of specific α-PD-1 (InVivoMAb anti-mouse PD-1 (CD276), clone 29 F.1A12) or α-B7-H3 (InVivoMAb antimouse B7-H3, clone MJ18) antibodies or their respective control IgG isotypes (InVivoMAb rat IgG2a isotype control,

anti-trinitrophenol, clone 2A3; InVivoMAb rat IgG1 isotype control, anti-horseradish peroxidase, clone HRPN) as indicated in Figures 3 and 4. All antibodies were purchased from BioXCell (West Lebanon, USA).

RNA isolation and reverse transcription (RT)-qPCR

Total lung RNA was isolated using peqGOLD TriFastTM reagent (VWR, Darmstadt, Germany) as previously described.[45] Purified RNA was transcribed into cDNA using the high-capacity cDNA reverse transcription kit (Thermo Fisher Scientific, Schwerte, Germany). Messenger RNA (mRNA) expression levels of single genes were determined by TaqMan RT-qPCR using the LightCycler 480 II (Roche Diagnostics, Mannheim, Germany). Each cDNA sample was normalized to the signal of the housekeeping gene transcripts of GAPDH and Cytochrome C (CytC). Sequences of primers used for RT-qPCR are listed in Supplementary Table 1.

Multiplex gene expression analysis was performed by hybridization of 100 ng of the isolated total lung RNA with code sets and subsequent analysis with the NanoString nCounter digital analyzer using the nCounter® PanCancer Immune Profiling Panel according to the manufacturer´s instructions. Data analysis was performed by the nSolver™ analysis software normalized to internally provided control genes.

Analysis immune cell phenotype via flow cytometry

To collect BALF immune cells, bronchoalveolar lavage (BAL) was performed as previously described.[19] Whole-lung immune cells were isolated by enzymatic digestion of left lungs of *cRaf-1-BxB* (*Raf-BxB*) or C57Bl/6 WT mice by using the mouse lung dissociation kit and gentle

MACS dissociator (Miltenyi, Bergisch Gladmach, Germany) according to the manufacturer's protocol.

After cell isolation via BALF or enzymatic digestion, erythrocytes were lysed and the cells were subsequently stimulated for 6 h with eBioscience™ Cell Stimulation Cocktail (plus protein transport inhibitors) (Thermo Fisher Scientific, Schwerte, Germany). Afterward cells were stained for multi-color flow cytometry analysis (Gallios, Beckmann Coulter).

Prior to specific staining all samples were treated with anti-Fcγ RII/III (BD Pharmingen, Heidelberg, Germany) antibody. Following extracellular surface marker staining, samples were fixed and permeabilized for staining of intracellular proteins using the eBioscience™ Foxp3/transcription factor staining buffer set (Thermo Fisher Scientific, Schwerte, Germany). The gating strategy to discriminate amongst the different immune cell subsets and their respective activation markers is exemplarily shown in supplementary Figures 2 and 3. Analysis of distinct immune cell populations was performed using the antibodies listed in supplementary Table 2.

Immunohistochemistry

The right lung of each mouse was fixed in 4% PFA and embedded in paraffin after dehydration. Paraffin sections of 4 μm were analyzed. Heat-mediated antigen retrieval was performed with 10 mM citric acid buffer (pH 6.0). Afterward lung sections were blocked with 10% FBS containing 0.1% Triton-X-100 for 30 min. Antigen-specific staining was performed by incubation with primary antibodies (α-SIGLEC5 (Siglec-F) antibody [abcam, ab198000]; α-CD276 (B7-H3) antibody [abcam, ab226256]; α-CD3ε antibody SP7 [Thermo Fisher, MA514524]; rabbit anti-human c-Raf [SP-63]) for 1 h at RT followed by species-specific biotinylated secondary antibody incubation for 30 min. The Vectastain ABC-AP Kit (Vector Laboratories, Cat. No.: AK-5000) was used for visualization of the stained proteins as described in the manufacturer´s protocol. Pictures were generated with the Biorevo BZ-9000 microscope (Keyence, Neu-Isenburg, Germany) and the Keyence BZ Analyzer software. For absolute quantification of tumor tissue, three different sections of each mouse lung (approx. 250 μm apart from each other) were quantified from 5 mice per treatment group. The area of the hRafBxB-positive tumor foci was quantified and expressed in relation to the total section area of each lung lobe by using the Keyence BZ Analyzer Software (Keyence). All analyses were quantified in a blinded manner.

Statistical analysis

Data is expressed as mean ± SEM. Statistical analysis was performed using GraphPad Prism software (version 6) and the following two-tailed tests: the Mann–Whitney U test when two groups were compared; One-Way ANOVA followed by Tukey´s comparison analysis when more than two groups were compared; 2-way ANOVA, followed by Sidak's or Dunn's multiple comparisons test when more than one parameter changed in the groups. Results were considered statistically significant at $P < .05$ and displayed as * $P < .05$, ** $P < .01$, *** $P < .001$, ****$P < .0001$. Mice were allocated randomly into experimental groups after matching for age and gender. Specific numbers of animals per group can be found in the corresponding figure legends.

Acknowledgments

Disclosure of interests

The authors declare no conflict of interest.

Funding

ORCID

Stephan Ludwig 🄓 http://orcid.org/0000-0003-4490-3052

References

1. Siegel RL, Miller KD, Jemal A; Siegel RL, Miller KD. Cancer statistics, 2019.. CA Cancer J Clin. 2019;69(1):7–34. doi:10.3322/caac.21551.

2. Jain P, Jain C, Velcheti V. Role of immune-checkpoint inhibitors in lung cancer. Ther Adv Respir Dis. 2018;12:1–13. doi:10.1177/https.

3. Prasad DVR, Nguyen T, Li Z, et al. Murine B7-H3 is a negative regulator of T cells. J Immunol. 2004;173(4):2500–2506. doi:10.4049/jimmunol.173.4.2500.

4. Chen C, Shen Y, Qu Q, Chen X, Zhang X, Huang J. Induced expression of B7-H3 on the lung cancer cells and macrophages suppresses T-cell mediating anti-tumor immune response. Exp Cell Res. 2013;319(1):96–102. doi:10.1016/j.yexcr.2012.09.006.

5. Lee YH, Martin-Orozco N, Zheng P, et al. Inhibition of the B7-H3 immune checkpoint limits tumor growth by enhancing cytotoxic lymphocyte function. Cell Res. 2017;27(8):1034–1045. doi:10.1038/cr.2017.90.

6. Huber S, Hoffmann R, Muskens F, Voehringer D. Alternatively activated macrophages inhibit T-cell proliferation by Stat6-dependent expression of PD-L2. Blood. 2010;116(17):3311–3320. doi:10.1182/blood-2010-02-271981.

7. Borghaei H, Paz-Ares L, Horn L, et al. Nivolumab versus docetaxel in advanced non-squamous nonsmall cell lung cancer. N Engl J Med. 2015;373(17):1627–1639. doi:10.1056/NEJMoa1507643. Nivolumab.

8. Herbst RS, Baas P, Kim DW, et al. Pembrolizumab versus docetaxel for previously treated, PD-L1positive, advanced non-small-cell lung cancer (KEYNOTE-010): a randomised controlled trial. Lancet. 2016;387(10027):1540–1550. doi:10.1016/S0140-6736(15)01281-7.

9. Rittmeyer A, Barlesi F, Waterkamp D, et al. Atezolizumab versus docetaxel in patients with previously treated non-small-cell lung cancer (OAK): a phase 3, open-label, multicentre randomized controlled trial. Lancet. 2017;389(10066):255–265. doi:10.1016/S0140-6736(16)32517-X.Atezolizumab.

10. Lynch TJ, Bondarenko I, Luft A, et al. Ipilimumab in combination with paclitaxel and carboplatin as first-line treatment in stage IIIB/IV non-small-cell lung cancer: results from a randomized, double-blind, multicenter phase II study. J Clin Oncol. 2012;30(17):2046–2054. doi:10.1200/JCO.2011.38.4032.

11. Sitnik S, Masemann D, Leite Dantas R, Wixler V, Ludwig S. PD-1 IC inhibition synergistically improves influenza a virus-mediated oncolysis of metastatic pulmonary melanoma. Mol Ther - Oncolytics. 2020 17(June;17:190–204. doi:10.1016/j.omto.2020.03.023.

12. Hamilton JR, Vijayakumar G, Palese P. A Recombinant Antibody-Expressing Influenza Virus Delays Tumor Growth in a Mouse Model.. Cell Rep. 2018;22(1):1–7. doi:10.1016/j.celrep.2017.12.025.

13. Kellish P, Shabashvili D, Rahman MM, et al. Oncolytic virotherapy for small-cell lung cancer induces immune infiltration and prolongs survival. J Clin Invest. 2019;129(6):2279–2292. doi:10.1172/JCI121323.

14. Durham NM, Mulgrew K, McGlinchey K, et al. Oncolytic VSV primes differential responses toimmuno-oncology therapy. Mol Ther. 2017;25(8):1917–1932. doi:10.1016/j.ymthe.2017.05.006.

15. Bourgeois-Daigneault MC, Roy DG, Aitken AS, et al. Neoadjuvant oncolytic virotherapy before surgery sensitizes triple-negative breast cancer to immune checkpoint therapy. Sci Transl Med. 2018;10(422):422. doi:10.1126/scitranslmed.aao1641.

16. Sivanandam V, LaRocca CJ, Chen NG, Fong Y, Warner SG. Oncolytic viruses and immune checkpointinhibition: the best of both worlds. Mol Ther - Oncolytics. 2019 June;13:93–106. doi:10.1016/j.omto.2019.04.003.

17. LaRocca CJ, Warner SG. Oncolytic viruses and checkpoint inhibitors: combination therapy in clinical trials. Clin Transl Med. 2018;7(1). doi:10.1186/s40169-018-0214-5.

18. Kerkhoff E, Fedorov LM, Siefken R, Walter AO, Papadopoulos T, Rapp UR. Lung-targeted expression of the c-Raf-1 kinase in transgenic mice exposes a novel oncogenic character of the wild-type protein. Cell Growth Differ. 2000;11:185–190.

19. Masemann D, Köther K, Kuhlencord M, et al. Oncolytic influenza virus infection restores immunocompetence of lung tumor-associated alveolar macrophages. Oncoimmunology. 2018;7(5):e1423171. doi:10.1080/2162402X.2017.1423171.

20. Pesce S, Greppi M, Grossi F, et al. PD/1-PD-Ls checkpoint: insight on the potential role of NK cells. Front Immunol. 2019 JUN;10:1–8. doi:10.3389/fimmu.2019.01242.

21. Hsu J, Raulet DH, Ardolino M, et al. Contribution of NK cells to immunotherapy mediated by PD-1/PD-L1 blockade graphical abstract find the latest version : contribution of NK cells to immunotherapy mediated by PD-1/PD-L1 blockade. J Clin Invest. 2018;128(10):4654–4668. doi:10.1172/JCI99317.

22. Rojas JJ, Sampath P, Hou W, Thorne SH. Defining effective combinations of immune checkpointblockade and oncolytic virotherapy. Clin Cancer Res. 2015;21(24):5543–5551. doi:10.1038/nbt.3121.ChIP-nexus.

23. Yonesaka K, Haratani K, Takamura S, et al. B7-H3 negatively modulates ctl-mediated cancerImmunity. Clin Cancer Res. 2018;24(11):2653–2664. doi:10.1158/1078-0432.CCR-17-2852.

24. Song J, Shi W, Zhang Y, Sun M, Liang X, Zheng S. Epidermal growth factor receptor and B7-H3 expression in esophageal squamous tissues correlate to patient prognosis. Onco Targets Ther. 2016;9:6257–6263. doi:10.2147/OTT.S111691.

25. Gainor JF, Shaw AT, L V S, et al. EGFR mutations and alk rearrangements are associated with low response rates to pd-1 pathway blockade in non-small cell lung cancer (NSCLC): a retrospective analysis. Clin Cancer Res. 2016;22(18):4585–4593. doi:10.1158/1078-0432.CCR-153101.EGFR.

26. Xia L, Liu Y, Wang Y. PD-1/PD-L1 blockade therapy in advanced non-small-cell lung cancer: current status and future directions. Oncologist. 2019;24(S1). doi:10.1634/theoncologist.2019-io-s1s05.

27. Ribas A, Dummer R, Puzanov I, et al. Oncolytic virotherapy promotes intratumoral T cell infiltration and improves anti-PD-1 immunotherapy. Cell. 2017;170(6):1109–1119.e10. doi:10.1016/j.cell.2017.08.027.

28. Zamarin D, Ricca JM, Sadekova S, et al. PD-L1 in tumor microenvironment mediates resistance to oncolytic immunotherapy. J Clin Invest. 2018;128(4):1413–1428. doi:10.1172/JCI98047.

29. Trefny MP, Kaiser M, Stanczak MA, et al. PD-1+ natural killer cells in human non-small cell lung cancer can be activated by PD-1/PD-L1 blockade. Cancer Immunol Immunother. 2020. doi:10.1007/s00262-020-02558-z.

30. Thommen DS, Koelzer VH, Herzig P, et al. A transcriptionally and functionally distinct pd-1 + cd8 + t cell pool with predictive potential in non-small-cell lung cancer treated with pd-1 blockade. Nat Med. 2018;24(7). doi:10.1038/s41591-018-0057-z

31. Platonova S, Cherfils-Vicini J, Damotte D, et al. Profound coordinated alterations of intratumoral NK cell phenotype and function in lung carcinoma. Cancer Res. 2011;71(16):5412–5422. doi:10.1158/00085472.CAN-10-4179.

32. Altan M, Pelekanou V, Schalper KA, et al. B7-H3 expression in NSCLC and its association with B7-H4, PD-L1 and tumor-infiltrating lymphocytes. Clin Cancer Res. 2017;22(1):5202–5209. doi:10.1158/10780432.CCR-16-3107.

33. Seo JS, Kim A, Shin JY, Kim YT. Comprehensive analysis of the tumor immune micro-environment in non-small cell lung cancer for efficacy of checkpoint inhibitor. Sci Rep. 2018;8(1):1–14. doi:10.1038/s41598-018-32855-8.

34. Sumitomo R, Hirai T, Fujita M, Murakami H, Otake Y. Huang C long. PD-L1 expression on tumorinfiltrating immune cells is highly associated with M2 TAM and aggressive malignant potential in patients with resected non-small cell lung cancer. Lung Cancer. 2019 June;136:136–144. doi:10.1016/j.lungcan.2019.08.023.

35. Yamazaki T, Akiba H, Iwai H, et al. Expression of programmed death 1 ligands by murine T cells andAPC. J Immunol. 2002;169(10):5538–5545. doi:10.4049/jimmunol.169.10.5538.

36. Arlauckas SP, Garris CS, Kohler RH, et al. mediated resistance pathway in anti-PD-1 therapy. Sci TranslMed. 2017;9(389):1–20. doi:10.1126/scitranslmed.aal3604.In.

37. Brigati C, Noonan DM, Albini A, Benelli R. Tumors and inflammatory infiltrates: friends or foes? ClinExp Metastasis. 2002;19 (3):247–258. doi:10.1023/A:1015587423262.

38. Muster T, Rajtarova J, Sachet M, et al. Interferon resistance promotes oncolysis by influenza virus NS1deletion mutants. Int J Cancer. 2004;110 (1):15–21. doi:10.1002/ijc.20078.

39. Bergmann M, Garcia-Sastre A, Carnero E, et al. Influenza virus NS1 protein counteracts PKR-mediated inhibition of replication. J Virol. 2000;74(13):6203–6206. doi:10.1128/JVI.74.13.6203-6206.2000.

40. Van Rikxoort M, Michaelis M, Wolschek M, et al. Oncolytic effects of a novel influenza a virus expressing interleukin-15 from the NS reading frame. PLoS One. 2012;7(5):e36506. doi:10.1371/journal.pone.0036506.

41. Vigdorovich V, Ramagopal UA, Lázár-molnár E, et al. Structure and T cell inhibition properties of B7 family member, B7-H3. Structure. 2013;21(5):707–717. doi:10.1016/j.str.2013.03.003.

42. Mao Y, Chen L, Wang F, et al. Cancer cell-expressed B7-H3 regulates the differentiation of tumor-associated macrophages in human colorectal carcinoma. Oncol Lett. 2017;24(S1):6177–6183. doi:10.3892/ol.2017.6935.

43. Zhang G, Wang J, Kelly J, et al. B7-H3 augments the inflammatory response and is associated withhuman sepsis. J Immunol. 2010;185 (6):3677–3684. doi:10.4049/jimmunol.0904020.

44. Seyer R, Hrincius ER, Ritzel D, et al. Synergistic adaptive mutations in the hemagglutinin and polymerase acidic protein lead to increased virulence of pandemic 2009 H1N1 influenza a virus in mice. J Infect Dis. 2012;205:262–271. doi:10.1093/infdis/jir716.

45. Börgeling Y, Schmolke M, Viemann D, Nordhoff C, Roth J, Ludwig S. Inhibition of p38 mitogenactivated protein kinase impairs influenza virus-induced primary and secondary host gene responses and protects mice from lethal H5N1 infection. J Biol Chem. 2014;289(1):13–27. doi:10.1074/jbc.M113.469239.